J. Fluid Mech. (2022), *vol*. 935, A11, doi:10.1017/jfm.2021.1160

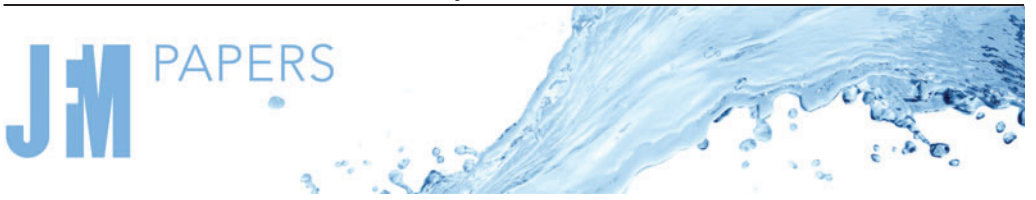

Propagation speed of turbulent fronts in pipe flow at high Reynolds numbers

Kaiwen Chen[1], **Duo Xu**[2,3] **and Baofang Song**[1,†]

[1]Center for Applied Mathematics, Tianjin University, Tianjin 300072, PR China

[2]The State Key Laboratory of Nonlinear Mechanics, Institute of Mechanics, Chinese Academy of Sciences, Beijing 100190, PR China

[3]School of Engineering Science, University of Chinese Academy of Sciences, Beijing 100049, PR China

(Received 27 June 2021; revised 10 December 2021; accepted 29 December 2021)

We investigated the propagation of turbulent fronts in pipe flow at high Reynolds numbers by direct numerical simulation. We used a technique combining a moving frame of reference and an artificial damping to isolate the fronts in short periodic pipes, which enabled us to explore the bulk Reynolds number up to $Re = 10^5$ with affordable computation power. We measured the propagation speed of the downstream front and observed that a fit of $1.971 - (Re/1925)^{-0.825}$ (in unit of bulk speed) captures this speed above $Re \simeq 5000$ very well. The speed increases monotonically as Re increases, in stark contrast to the decreasing trend above $Re \simeq 10\,000$ reported by Wygnanski & Champagne (*J. Fluid Mech.*, vol. 59, 1973, pp. 281–335). The speed of the upstream front overall agrees with the former studies and $0.024 + (Re/1936)^{-0.528}$ fits our data well, and those from the literature. Based on our analysis of the front dynamics, we proposed that both front speeds would keep their respective monotonic trends as the Reynolds number increases further. We show that, at high Reynolds numbers, the local transition at the upstream front tip is via high-azimuthal-wavenumber structures in the high-shear region near the pipe wall, whereas at the downstream front tip is via low-azimuthal-wavenumber structures in the low-shear region near the pipe centre. This difference is possibly responsible for the asymmetric speed scalings between the upstream and downstream fronts.

Key words: shear-flow instability, transition to turbulence, pipe flow

1. Introduction

At sufficiently high Reynolds numbers, once perturbed locally, pipe flow becomes turbulent and develops two turbulent fronts on the upstream and downstream (Lindgren 1957; Wygnanski & Champagne 1973). The turbulent region expands via the propagation

† Email address for correspondence: baofang_song@tju.edu.cn

of the two fronts and, therefore, the dynamics of the fronts determines how the laminar flow is entrained into the turbulent region and how fast the turbulent region can expand. Since Lindgren (1957), many studies have been devoted to studying turbulent fronts in straight and bent pipes over the past decades (Lindgren 1969; Wygnanski & Champagne 1973; Durst & Ünsal 2006; Nishi *et al.* 2008; Duguet, Willis & Kerswell 2010; Holzner *et al.* 2013; Barkley *et al.* 2015; Song *et al.* 2017; Rinaldi, Canton & Schlatter 2019), among which the global propagation speed of the fronts has been an important subject.

A few studies attempted to theoretically derive the front speed. For the upstream front (UF), by analysing the energy flux across a control volume enclosing the entire front region (the part between the parabolic laminar flow on the upstream and fully developed turbulent flow on the downstream), Lindgren (1969) derived an asymptotic speed of 0.69 in theory, and speculated 0.64 being a lower limit of the speed in experiments as $Re \to \infty$. However, as Wygnanski & Champagne (1973) pointed out, these values are rather far away from experimental measurements at high Reynolds numbers, and a trend approaching these values was not supported by the measurements. Treating the front as an isosurface of a proper quantity (e.g. the enstrophy), Holzner *et al.* (2013) theoretically derived the local speed of the three-dimensional isosurface relative to the local flow speed, and evaluated the contributions from different physical mechanisms. Given the local flow speed, one can in principle calculate an instantaneous axial propagating speed of the isosurface as a whole. However, as the authors pointed out, the method requires fully resolving the complex highly convoluted isosurfaces and is challenging to implement for both numerical simulations and experiments. Besides, the method requires detailed local flow speed at the isosurface to calculate the global propagation speed of the isosurface.

Regarding the local transition mechanisms at the fronts, qualitatively, instabilities associated with low-speed streaks were proposed for the UF of turbulent puffs (localised turbulence with an approximately constant axial extension) and slugs (turbulent structures expanding along the pipe axis) at low and moderate Reynolds numbers (Shimizu & Kida 2009; Duguet *et al.* 2010; Hof *et al.* 2010). However, to our knowledge, there still lacks a quantitative understanding of the mechanism. As a result, predicting the front speed theoretically from first principles has not been realised, and determining the propagation speed by tracking the front remains the main approach in either experiments or numerical simulations.

Figure 1 presents some important studies on the global propagation speed of the fronts, in which the bulk Reynolds number is defined as $Re = UD/\nu$ with U being the bulk speed (axial velocity averaged in the pipe cross-section), D the pipe diameter and ν the kinematic viscosity of the fluid. We use this definition of the Reynolds number, and normalise length by D and speed by U in this paper. It can be seen that the data sets for the UF speed roughly agree with each other, whereas they show much scattering for the downstream front (DF) speed. What is more, relevant study at high Reynolds numbers ($\gtrsim$10 000) is rare.

Among the studies, Wygnanski & Champagne (1973) carried out a comprehensive investigation into the kinematics and structure of the fronts, and considered the highest Reynolds number so far (up to $Re \simeq 60\,000$). In fact, to our knowledge, their work was the only one that covers the regime of $Re \gtrsim 10\,000$. Based on their measurements, the authors concluded that the speeds of both the UF and DF decrease as Reynolds number increases above $Re \simeq 10\,000$ such that the difference between the two, i.e. the expansion rate of the turbulent region, approaches the bulk speed U as $Re \to \infty$ (see figure 1). However, the basic laminar flow had not fully developed in their pipe at high Reynolds numbers (indicated by their figure 9). Therefore, the front speeds they reported at high Reynolds numbers were likely affected by the insufficiently developed basic flow, although

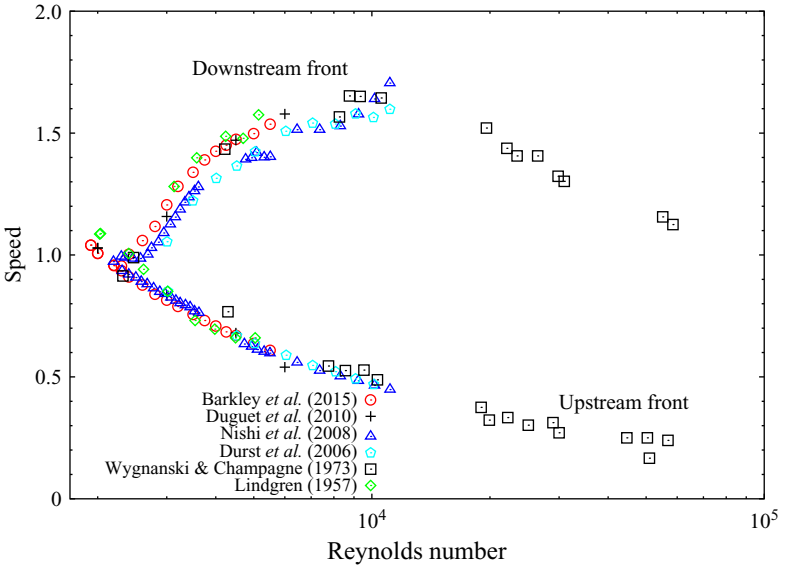

Figure 1. Global axial propagation speed as a function of the bulk Reynolds number taken from the literature.

they didn't explain the mechanism responsible for the decreasing trend of the DF speed above $Re \simeq 10\,000$. Barkley *et al.* (2015) and Barkley (2016) presented a state-of-the-art study on the fronts in the transitional Reynolds number regime ($Re < 6000$) by combining experiments, numerics and theoretical modelling. Their advection–reaction–diffusion model describes the front dynamics and kinematics on large-scale in the transitional regime well. Based on the usual one-dimensional representations of the flow along the pipe axis (see e.g. Nishi *et al.* (2008), Duguet *et al.* (2010) and Song *et al.* (2017)), Barkley *et al.* (2015) and Barkley (2016) assumed that the UF and DF gradually become the mirror image of each other as Re increases, and predicted that the front speeds will be antisymmetric about the advection speed of the bulk turbulence at high Re. Their prediction implied that the DF speed would monotonically increase as Re increases, conflicting with the measurements of Wygnanski & Champagne (1973). However, their model analysis was only informed by data (both experimental and numerical) up to $Re \simeq 6000$, therefore, it is unclear if the model quantitatively describes the fronts at high Reynolds numbers.

In a word, there has been no consensus on the kinematics of the DF at high Reynolds numbers. One difficulty in measuring the front speed at high Reynolds numbers in experiments, especially for the DF, is that the speed takes a long time to saturate given usual initial perturbations (e.g. transverse jets and impulsive partial blockage) so that the pipe should be sufficiently long for the DF to develop. Nishi *et al.* (2008) used a $533D$ (8 m) pipe and found that the DF speed experiences long transients and the higher the Reynolds number, the longer the transient. They only performed measurements up to $Re = 11\,000$. Wygnanski & Champagne (1973) used a $500D$ pipe to measure the front speed up to $Re \simeq 60\,000$. However, they didn't show the development of the front speed with time and, therefore, whether or not the front speed had saturated is not clear (it probably had not at high Reynolds numbers because the basic flow was still developing at their measurement point). A second difficulty, which is possibly more difficult to overcome, is that small environmental disturbances may trigger turbulence at high Reynolds numbers and affect the fronts (Hof, Juel & Mullin 2003; Peixinho & Mullin 2007). Indeed, Wygnanski & Champagne (1973) noticed increasing low-frequency oscillations as Re increases in their

basic flow, which may also contribute to the deviation of the basic flow from the parabolic laminar flow.

In numerical simulations, environmental disturbances can be kept low and periodic pipes can keep the front from exiting the pipe; however, the fast growth of slugs at high Reynolds numbers quickly renders the pipe fully turbulent if the pipe is not sufficiently long. Song (2014) (see their figure 5 of Chapter 3) reported that, by using localised puffs as the initial perturbation (the turbulent core is approximately $10D$ long), the pipe length needed to obtain a saturated DF speed increases as Re increases. For example, at $Re = 3000$, the DF speed saturates as slugs grow to a length of approximately $30D$, whereas this length grows nearly linearly to $80D$ at $Re = 4250$ and to $125D$ at $Re = 5500$. Therefore, the pipe length should be significantly longer than $125D$ for $Re = 5500$ (Song (2014) used a 180-D pipe). At higher Reynolds numbers, the pipe length, and consequently the computational cost, grows rapidly. As an estimate, for direct numerical simulation (DNS) that uses uniform grids in the axial and azimuthal directions, a $250D$-long pipe for $Re = 10\,000$ needs approximately 5×10^8 grid points, and this number grows to approximately 1×10^{10} for $Re = 40\,000$. Besides the increasing number of grid points, the decreasing time step size and increasing time for the speed to saturate as Re increases also make the DNS study in the normal approach infeasible.

In this work, we measure the global axial propagation speed of the fronts using a technique combining a moving frame of reference and an artificial damping in relatively short periodic pipes to isolate individual fronts. Besides, by using the well-developed fronts simulated at close Reynolds numbers as initial conditions, the initial adjustment of the flow can be drastically shortened. These strategies circumvent the aforementioned difficulties and enable us to investigate turbulent fronts at unprecedentedly high Reynolds numbers using DNS.

2. Methods

2.1. *Numerical methods*

We solve the incompressible Navier–Stokes equations in a moving frame of reference with a streamwise speed of c and an artificial damping term with the form of $-\beta(z)\boldsymbol{u}$, i.e.

$$\frac{\partial \boldsymbol{u}}{\partial t} + (\boldsymbol{u} + c) \cdot \boldsymbol{\nabla} \boldsymbol{u} = -\boldsymbol{\nabla} p + \frac{1}{Re} \nabla^2 \boldsymbol{u} - \beta(z)\boldsymbol{u}, \quad \boldsymbol{\nabla} \cdot \boldsymbol{u} = 0, \tag{2.1}$$

where $\boldsymbol{u}$ is the velocity with respect to the moving frame of reference and p the pressure. The volume flux (the bulk speed) is kept constant during the simulation. The form of the damping term is inspired by Kanazawa (2018). The equations are solved in cylindrical coordinates (r, θ, z), which represent radial, azimuthal and streamwise coordinates, respectively. We use the open-source pipe flow code Openpipeflow (Willis & Kerswell 2009; Willis 2017) to perform the simulations. As β is dependent on z, the damping term is treated as a nonlinear term in the time stepping. The resolutions for all simulations performed in this paper are listed in the Appendix.

The moving frame of reference and damping term play the role of tracking and isolating a front or even a part of a front in a short pipe domain, such that we can explore the high Re regime. This strategy is only justified if the front is locally self-sustained and does not depend on the flow far from it. This is true for the fronts of strong slugs according to Barkley *et al.* (2015), Barkley (2016) and Song *et al.* (2017), and will also be evidenced later in this paper. The DF of puffs and weak slugs at low Reynolds numbers is not self-sustained, to which our technique may not apply. The damping coefficient β is a

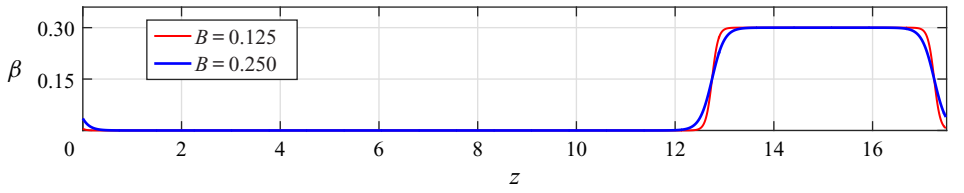

Figure 2. The damping coefficient β with $A = 0.3$, $z_0 = 15$ and $R = 2.25$. The thin red line is for $B = 0.125$ and the bold blue line is for $B = 0.25$. Note that a periodic boundary condition is considered for β.

function of only the axial coordinate and will be used to confine the damping effect in only a part of the pipe. Specifically, we choose the following form:

$$\beta(z) = A\left(0.5 - 0.5\tanh\left(\frac{|z - z_0| - R}{B}\right)\right), \tag{2.2}$$

where A is the amplitude, R the nominal half-width of the damping region and B controls the steepness of the decay of the damping at the boundary of the damping region. Therefore, this coefficient localises the damping roughly in a region of $z_0 - R < z < z_0 + R$. Ideally, the speed of the moving frame c should be set to the speed of the front, which, however, is not known *a priori*. Therefore, c is first estimated (e.g. using the front speed measured at a close Re) and then adjusted dynamically in run time, so that the axial location of the front does not change significantly. Figure 2 shows the shape of β given $A = 0.3$, $z_0 = 15$ and $R = 2.25$ with $B = 0.25$ (the thin red line) and with $B = 0.125$ (the bold blue line).

3. Speed measurements

3.1. *Validation*

First, we validate our technique by comparing the front speed for $Re = 5000$ with the data of Barkley *et al.* (2015) and Song *et al.* (2017) which were obtained in long stationary periodic pipes. The system setting is characterised by the pipe length L, a reference position of the front z_{f0} and damping parameters z_0, R, A and B as defined in (2.2). For locating the front in the axial direction, following Song *et al.* (2017), we set a threshold in the cross-sectional kinetic energy (KE),

$$q(z) := \int_0^1 \int_0^{2\pi} (u_r^2 + u_\theta^2) r \,\mathrm{d}\theta \,\mathrm{d}r, \tag{3.1}$$

above which the flow is considered sufficiently turbulent. As Song (2014) and Song *et al.* (2017) reported, the specific value of this threshold would not affect the average front speed as long as it is in a reasonable range.

Figure 3 shows a set-up for the DF at $Re = 5000$ with a pipe length $L = 17.5$ (see the parameters in table 1). We aim to keep the axial location of the front at around $z_{f0} = 5$. The damping coefficient β is set as that shown in figure 2. This set-up gives approximately a $7D$-long laminar gap between the front and the damping region. Figure 3(a) shows a snapshot of the front in the r–z cross-section, and figure 3(b) shows $q(z)$ along the pipe axis. With an estimation of the front speed $c_0 = 1.50$, the axial location of the front z_f is determined using the threshold 5×10^{-4} in q approximately every $\delta t = 6.25D/U$, see figure 4(a). Subsequently the speed of the frame of reference c is dynamically adjusted

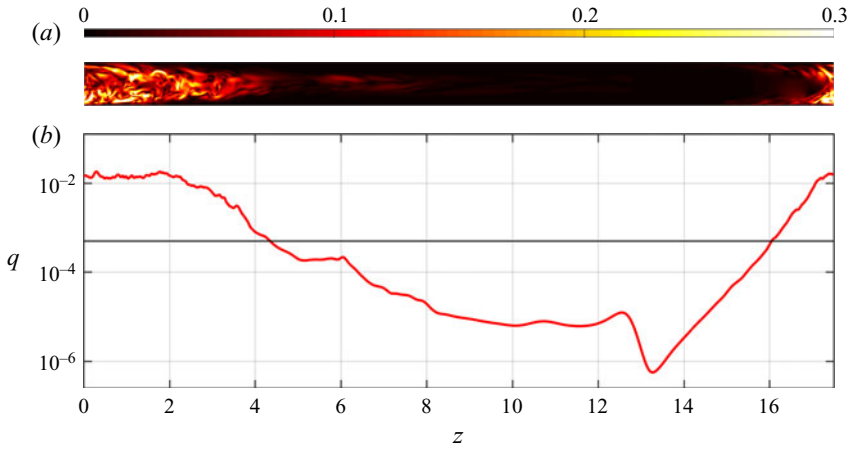

Figure 3. The parameter setting of $L = 17.5$, $z_{f0} = 5$, $z_0 = 15$, $R = 2.25$, $A = 0.3$ and $B = 0.25$ for $Re = 5000$. The estimated front speed $c_0 = 1.50$. The damping coefficient β with these parameters is exactly the one shown in figure 2. (*a*) One snapshot of the front in the r–z cross-section, in which the transverse velocity $\sqrt{u_r^2 + u_\theta^2}$ is colour-coded. The front is on the left (upstream) and the damping region is on the right (downstream), with the laminar gap in between (the dark region). (*b*) The quantity q defined in (3.1) is plotted along the pipe axis at a time instant (red bold line). The horizontal black thin line marks the threshold by which the location of the front is determined. The nominal axial position of the front is $z_f = 4.3$ at this time instant, given by the left intersection between the red curve and black line.

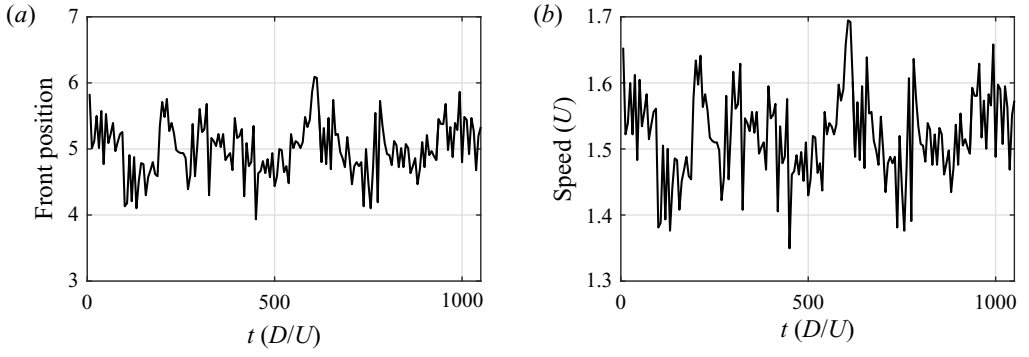

Figure 4. (*a*) The nominal axial position of the front, determined by the threshold in q as described in the caption of figure 3, for the DF at $Re = 5000$. (*b*) The speed of the frame of reference as a function of time.

according to the location of the front as

$$c + (z_f - z_{f0})/\delta t \to c, \tag{3.2}$$

so that the front does not move too far away from the reference position $z_{f0} = 5$, see figure 4. Note that other values of δt can be chosen as long as the position of the front does not fluctuate much. As shown in the figure, this technique indeed can isolate the front and track it for a very long time (a time window of approximately 1050 D/U is shown in the figure) in the $17.5D$ pipe.

As the location of the front only fluctuates slightly around $z_{f0} = 5$ (within $1D$) in the moving frame of reference over a long time, we can approximate the front speed as the average speed of the frame of reference. In this test, the average of c is approximately 1.518. To show the effect of the pipe length to the front speed, we also measured the

	Re	L	z_{f0}	z_0	R	A	B	threshold	max Δt	T	speed
DF	5000	17.5	5	15	2.25	0.3	0.25	5×10^{-4}	2.0×10^{-3}	1050	1.518
	5000	35	11.5	29	3.5	0.1	0.5	5×10^{-4}	2.0×10^{-3}	1250	1.520
UF	5000	17.5	10.5	5.0	4.5	0.1	0.25	5×10^{-4}	1.25×10^{-3}	400	0.630

Table 1. Pipe length, damping parameter setting, threshold in q, time step size and averaging time of the speed for the DF at $Re = 5000$.

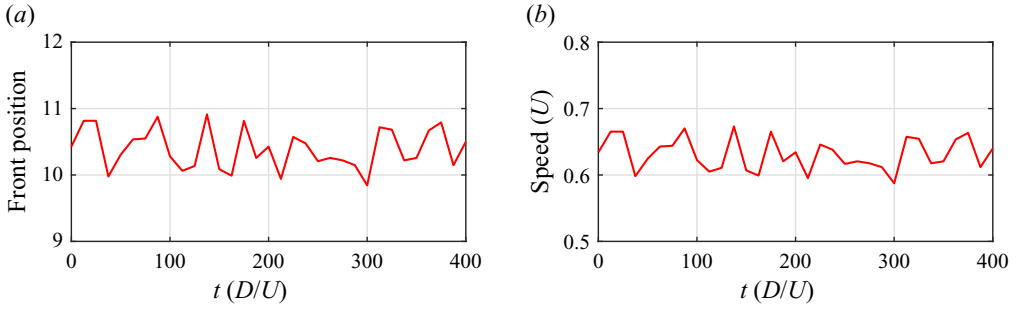

Figure 5. (a) The nominal axial position of the UF with the threshold of 5×10^4 in q (see table 1) at $Re = 5000$ in the $17.5D$ pipe. (b) The speed of the frame of reference.

speed in a $35D$ pipe with the parameters shown in table 1, which gives a laminar gap of approximately $14D$. The measurement gives 1.520 averaged over $1250D/U$, which is very close to the speed measured in the $17.5D$ pipe. Therefore, it seems that the speed measured in our simulations is not significantly affected by the pipe length as well as the spatial extension and strength of the damping. The speed of the DF measured in a $180D$ pipe by Barkley *et al.* (2015) and Song *et al.* (2017) is 1.498, which agrees with our current result within an error of approximately 1.3 %. The speed of the UF for $Re = 5000$ is also measured in the $L = 17.5D$ pipe with the parameters shown in table 1. The speed is 0.630 averaged over $400D/U$ (see figure 5), while Barkley *et al.* (2015) and Song *et al.* (2017) reported 0.637 in a $180D$ pipe. The speed was measured in a shorter time window than the DF because Nishi *et al.* (2008) and Song (2014) both reported that the speed of the UF stabilises much more quickly and fluctuates much more weakly than that of the DF, which was indeed also observed in the present work (to compare the fluctuations of the front position and frame speed in figures 4 and 5). Table 1 summarises the parameters and measured front speeds of these tests.

These tests suggest that this technique indeed enables us to study turbulent fronts in short periodic pipes without significant domain size effect. Besides serving as a validation, the results shown here also suggest that the front is indeed locally self-sustained and does not depend on the turbulent flow far from it, as the front speed does not change if the turbulence sufficiently far from it is damped. It should be noted that, the total observation time ($1050D/U$) of the well-developed DF in this $17.5D$ pipe based on a single run is roughly the same as the sum of the observation time of Song (2014) based on 20 runs with different puffs as initial conditions in a $180D$ pipe. In comparison, the computational cost is greatly reduced by using this technique.

	Re	L	z_{f0}	z_0	R	A	B	threshold	max Δt	T	speed
DF	7500	17.5	5	15	2.25	0.30	0.25	5×10^{-4}	1.25×10^{-3}	1000	1.650
	10 000	17.5	6	15	2.25	0.35	0.25	5×10^{-4}	1.25×10^{-3}	1350	1.710
	17 500	17.5	5	15	2.25	0.35	0.25	5×10^{-4}	1.00×10^{-3}	390	1.793
	25 000	17.5	5	15	2.25	0.35	0.25	5×10^{-4}	5.00×10^{-4}	180	1.867
	25 000	17.5	9	15	2.25	0.35	0.25	5×10^{-4}	6.25×10^{-4}	180	1.847
	40 000	17.5	9	15	2.25	0.35	0.25	5×10^{-4}	3.00×10^{-4}	100	1.877
UF	7500	17.5	10.5	4.75	4.25	0.30	0.25	5×10^{-4}	1.25×10^{-3}	750	0.511
	10 000	17.5	10.5	4.75	4.25	0.30	0.25	5×10^{-4}	1.25×10^{-3}	500	0.447
	17 500	17.5	10.5	5.5	2.5	0.35	0.25	5×10^{-4}	5.00×10^{-4}	100	0.343
	25 000	17.5	10.5	5.5	2.5	0.35	0.25	5×10^{-4}	3.10×10^{-4}	100	0.290
	40 000	17.5	10.5	5.5	2.5	0.35	0.25	5×10^{-4}	1.25×10^{-4}	25	0.233

Table 2. Reynolds number, damping parameters, threshold in q, time step size and averaging time of the speed for the DF (top) and UF (bottom) in the 17.5D pipe. All parameter settings assure that q drops by at least four orders of magnitude as turbulence passes the damping region and that q drops away from the front naturally by approximately four orders of magnitude (see the example for $Re = 5000$ in figure 3). Two settings of z_{f0} are compared for the DF at $Re = 25\,000$, which differ by approximately 1 % on the front speed.

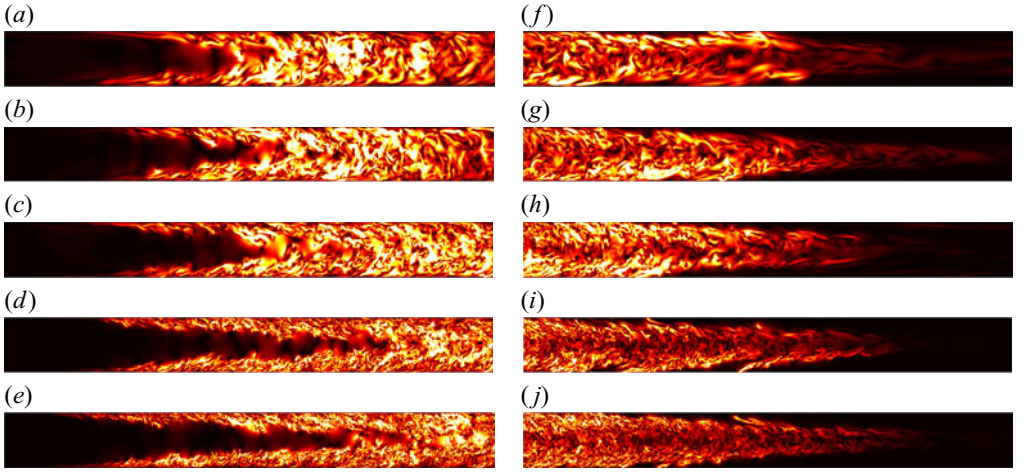

Figure 6. Fronts as Re increases: (a–e) UF; (f–j) DF. The Reynolds numbers (a, f–e, j) are 5000, 7500, 10 000, 25 000 and 40 000, respectively. A 9D-long pipe section is shown.

3.2. *Fronts at high Reynolds numbers*

With the parameter settings for the 17.5D pipe as shown in table 2, we simulated the fronts and measured the front speed up to $Re = 40\,000$. The structure of the fronts at several Reynolds numbers ranging from 5000 to 40 000 are visualised in figure 6. Overall, as Re increases, the front regions on both the upstream and downstream become longer in the axial direction, i.e. visually the fronts become more slender and reach farther into the laminar region. The measured speeds are shown in table 2.

However, at $Re = 40\,000$ the number of grid points becomes very large even for the 17.5D pipe, which reaches approximately 8.5×10^8. The other restricting factor is the rapidly decreasing time step size. Our time step size controller gives approximately

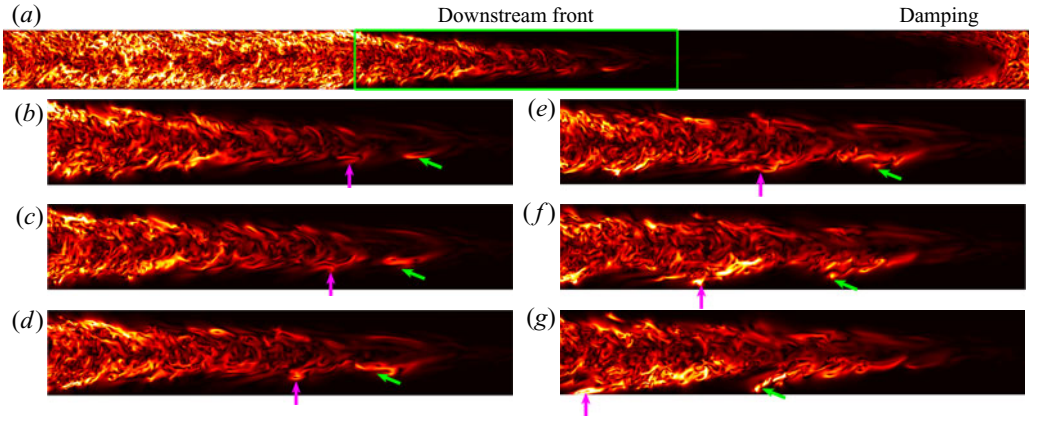

Figure 7. Visualisation of local transition at the DF at $Re = 25\,000$ in the moving frame of reference. (*a*) A snapshot of the cross-stream velocity $\sqrt{u_r^2 + u_\theta^2}$ in the z–r plane of the $17.5D$ pipe. Panels (*b–g*) show the flow in the region enclosed by the green rectangle in panel (*a*) at several time instants. Consecutive panels are separated by $0.875D/U$. In panels (*b–g*), vertical arrows and tilted arrows mark two local transition events.

$1.25 \times 10^{-4} D/U$ to assure convergence for simulating the UF and $2.5 \times 10^{-4} D/U$ for simulating the DF, given the same grid resolution setting, due to the explicit treatment of the damping term in the time stepping. Therefore, the computational cost becomes so high that we can only afford to measure the DF speed over a time window of $100D/U$ and the UF speed over a time window of $25D/U$. In order to obtain reliable statistics of the front speed at $Re = 40\,000$ and to consider higher Re, we had to reduce the pipe length further to reduce the cost.

The following observation suggests that further reduction in the pipe length is possible. Figure 7(*a*) visualises the DF at $Re = 25\,000$ simulated in a $17.5D$ pipe. The flow inside the green rectangle enclosing a part of the DF is visualised at a few time instants in figure 7(*b–g*). Local transition to turbulence at the tip of the front (close to the pipe centre) can be observed, see the evolution of the flow structures pointed to by the vertical and tilted arrows in figure 7(*b–g*). Initiating near the pipe centre, these structures appear to be stretched, and strengthen while extending toward the high shear region near the pipe wall. The slowing down (moving to the left) of the structures while approaching the wall, mainly due to the decreasing local flow speed, is clearly indicated by the axial locations of their upstream tips (see the arrows) in this frame of reference comoving with the DF. In fact, because of the radial turbulent momentum transport, the generated turbulent fluctuations will also extend toward the pipe centre and be advected downstream by the high speed flow at the pipe centre. This possibly triggers successive local transitions at the tip of the DF. However, as the flow is already turbulent near the pipe centre, this feedback process cannot be clearly seen; see supplementary movie 1 available at https://doi.org/10.1017/jfm.2021.1160 for more detailed dynamics at the DF. At the UF, similar local self-sustaining scenario was observed as shown in figure 8, but the difference is that the local transition initiates in the near-wall region. The generated turbulent fluctuations feedback the near-wall region and also extend toward the pipe centre and speed up due to the increasing local flow speed. The turbulence eventually merges at the pipe centre, filling the whole pipe cross-section; see supplementary movie 2 for more details. (We will revisit the transition scenario at the front tips in § 4.2.) Shimizu & Kida (2009) and Duguet *et al.* (2010) reported similar processes at the UF of puffs and slugs at much lower Reynolds numbers. According to this

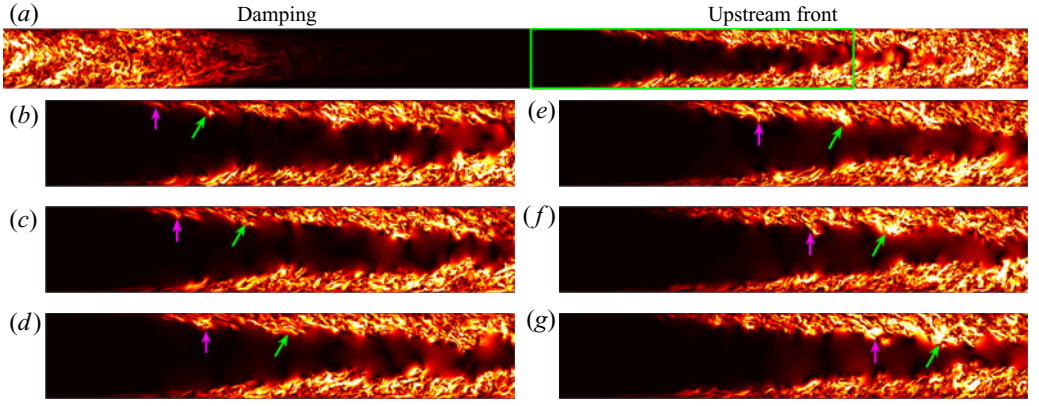

Figure 8. Visualisation of local transition at the UF at $Re = 25\,000$ in the moving frame of reference. The same quantity as in figure 7 is plotted. In panels (b–g), consecutive panels are separated by $0.625D/U$.

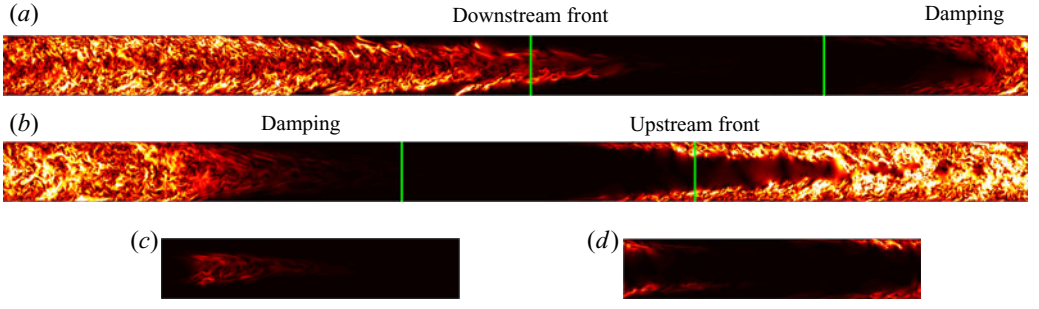

Figure 9. The $L = 17.5D$ pipe (a,b) and the $5D$ pipe (c,d) at $Re = 25\,000$. Panel (a) shows the DF and panel (b) shows the UF. The vertical green lines in each panel enclose the part of the front that we isolate by using the $5D$ periodic pipe, as shown in panels (c,d), respectively. The colourmap shows transverse velocity $\sqrt{u_r^2 + u_\theta^2}$ in the r–z cross-section. The specific damping parameters are listed in table 2 ($17.5D$ pipe) and table 3 ($5D$ pipe). Supplementary movie 3 and 4 show the flow in the $5D$ pipe at the DF and UF, respectively.

scenario, we speculate that the transition process is locally self-sustained at the front tips and does not depend on the flow sufficiently far away. This localness makes further pipe length reduction possible.

We reduced the pipe length further to $L = 5D$ to isolate the front tip; see the illustration in figure 9 for $Re = 25\,000$ (see also supplementary movies 3 and 4). This also relieves the restriction on the grid spacing and time step size because the flow is relatively less turbulent at the very tip of the fronts (see the Appendix). The front speeds are measured for $Re = 17\,500$ and $Re = 25\,000$ again for validation (see table 3). At $Re = 17\,500$, the averaging time for the DF is the same as in the $17.5D$ pipe, whereas at $Re = 25\,000$ the averaging times are significantly enlarged (see tables 2 and 3). For these two Reynolds numbers, we obtained very close speeds in the two pipes for both the UF and DF, justifying the use of the $5D$ pipe at least for the speed measurement (see tables 2 and 3). We were able to significantly increase the averaging time of the front speeds for $Re = 40\,000$ and, surprisingly, obtained very close values to those averaged over much shorter times in the $17.5D$ pipe. This suggests that the saturated front speeds at high Re do not fluctuate significantly with time, as Song (2014) reported. We then further measured the DF speed at $Re = 60\,000$ and 10^5 and the UF speed at $Re = 60\,000$ (see table 3).

	Re	L	z_{f0}	z_0	R	A	B	threshold	max Δt	T	speed
DF	17 500	5	1.75	4.375	1.125	0.4	0.1	1×10^{-4}	1.0×10^{-3}	390	1.808
	25 000	5	1.25	4.375	1.125	0.4	0.1	1×10^{-4}	7.5×10^{-4}	400	1.853
	40 000	5	1.75	4.375	1.125	0.4	0.1	1×10^{-4}	7.5×10^{-4}	250	1.893
	40 000	5	1.25	4.375	1.125	0.5	0.1	1×10^{-4}	7.5×10^{-4}	100	1.890
	60 000	5	1.75	4.375	1.125	0.4	0.1	1×10^{-4}	4.0×10^{-4}	150	1.913
	100 000	5	1.25	4.375	1.125	0.4	0.1	1×10^{-4}	3.0×10^{-4}	100	1.930
UF	17 500	5	3.5	1.375	1.375	0.5	0.1	1×10^{-4}	5.0×10^{-4}	200	0.332
	25 000	5	3.5	1.375	1.375	0.5	0.1	1×10^{-4}	5.0×10^{-4}	200	0.287
	40 000	5	3.5	1.375	1.375	0.5	0.1	1×10^{-4}	3.75×10^{-4}	100	0.225
	60 000	5	3.5	1.375	1.375	0.5	0.1	1×10^{-4}	2.5×10^{-4}	55	0.187

Table 3. The Reynolds number, damping parameters, threshold in q, time step size and averaging time of the speed for the DF (top) and UF (bottom) in the $5D$ pipe. Two settings for z_{f0} are compared for the DF at $Re = 40\,000$.

3.3. *The scaling of the front speed at high Reynolds numbers*

Figure 10 concludes the front speeds we measured with a comparison with most relevant data from the literature, which are also shown in figure 1. The major difference with the former data sets is that our results give an increasing trend for the DF speed up to $Re = 10^5$, whereas Wygnanski & Champagne (1973) gave the opposite trend above $Re \simeq 10\,000$. Besides, our data exhibit less scattering.

Intuitively, the DF is not expected to propagate faster than the centreline velocity of the basic laminar flow and, also, the UF is not expected to propagate upstream in the laboratory frame of reference against the advection by the basic flow. Based on our results, we expect both speeds to keep monotonic with Re and asymptotically approach some values in the range $[0, 2]$ as Re increases. We seek for a scaling of the form $a + bRe^c$ for both front speeds, suggested by the model analysis of Barkley *et al.* (2015). With the data for $Re = 5000$ in table 1, for $Re = 7500$ and 10 000 in table 2, and for $Re = 17\,500$ to 10^5 in table 3, we obtained best fits with the least square errors and slightly reformulated the scalings as

$$c_{DF} \approx 1.971 - (Re/1925)^{-0.825}, \tag{3.3}$$

$$c_{UF} \approx 0.024 + (Re/1936)^{-0.528}, \tag{3.4}$$

where c_{DF} denotes the DF speed and c_{UF} the UF speed. These two scalings are plotted as black solid curves in figure 10(*b*), which can be seen to fit our data (red filled circles) very well. Besides, the scaling of the c_{UF} (3.4) also fits the data from the literature very well. One can notice that the scaling of c_{DF} also fits the data from Barkley *et al.* (2015) down to $Re \simeq 3500$ well, while deviations are observed at lower Re. This can be expected because the fit (3.3) is based on data for strong fronts at high Re, while the DF is weak below $Re \simeq 2900$ and the transition from weak DF to strong DF completes close to $Re \simeq 3500$ according to Song *et al.* (2017).

4. Discussion

Barkley *et al.* (2015), by theoretical modelling and asymptotic analysis in a model system, proposed that, in the limit of an asymptotically strong front, the speeds of both fronts obey

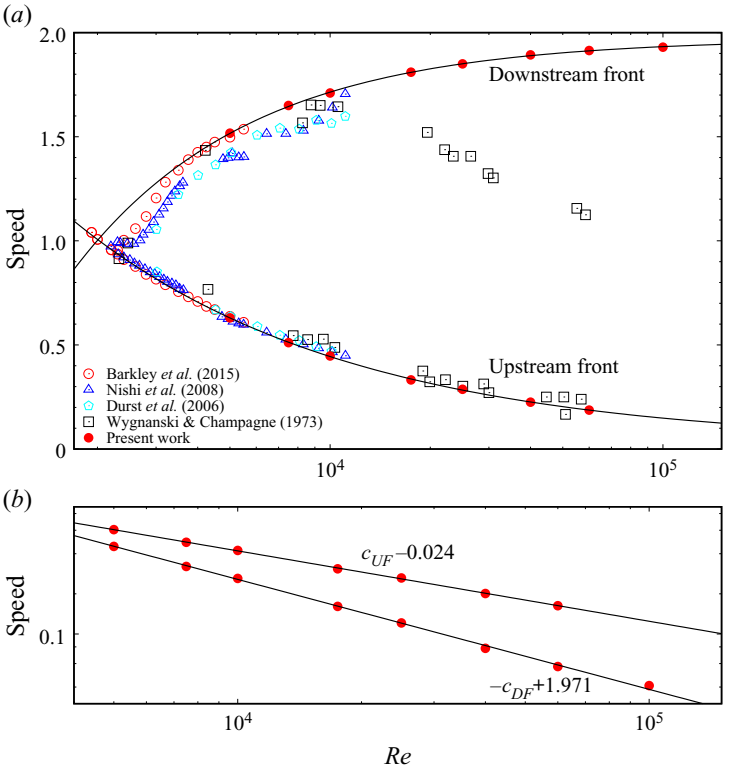

Figure 10. (*a*) Front speed as a function of *Re*. Some data sets from figure 1 are repeated here for comparison. (*b*) Our data (symbols) plotted in log–log scale. Lines show the fits (3.3) and (3.4).

the scaling of $a + bRe^{-0.5}$, where a and b are constants and are different for the UF and DF. Their DNS and experimental data up to $Re = 5500$ in long pipes showed that the UF speed seems to approximately follow this scaling. Their data for the DF in the strong front regime (above $Re \simeq 3500$) seem to follow this scaling also. However, the *Re* range for assessing the scaling is too narrow (from 3500 to 5500). Here, our simulations up to $Re = 60\,000$ for the UF show that the UF speed indeed closely follows the scaling proposed by Barkley *et al.* (2015) based on data in a much smaller *Re* range, but the DF speed approximately follows (3.3) from $Re = 5000$ to 10^5, in which the power considerably deviates from -0.5. This disagreement suggests that their assumption that the UF and DF become the mirror image of each other at high *Re* may not hold in real pipe flow.

Undoubtedly, results in the *Re* regime of the present work may not be simply extrapolated to infinite *Re*, and we are not proposing the scalings (3.3) and (3.4) as the asymptotic scalings as $Re \to \infty$. Besides, our results for high *Re* are based on measurements over $O(100)$ time units. Although the results of Song (2014) showed that the fluctuation of the front speed decreases as *Re* increases, and therefore the front speed measured in a reasonably long time interval will be increasingly representative as *Re* increases, we cannot rule out the possibility of considerable migration over larger time spans in the front speed (especially for the DF). Nonetheless, in the following, we propose that the monotonicity of the characteristic speed of both fronts will persist as *Re* increases further.

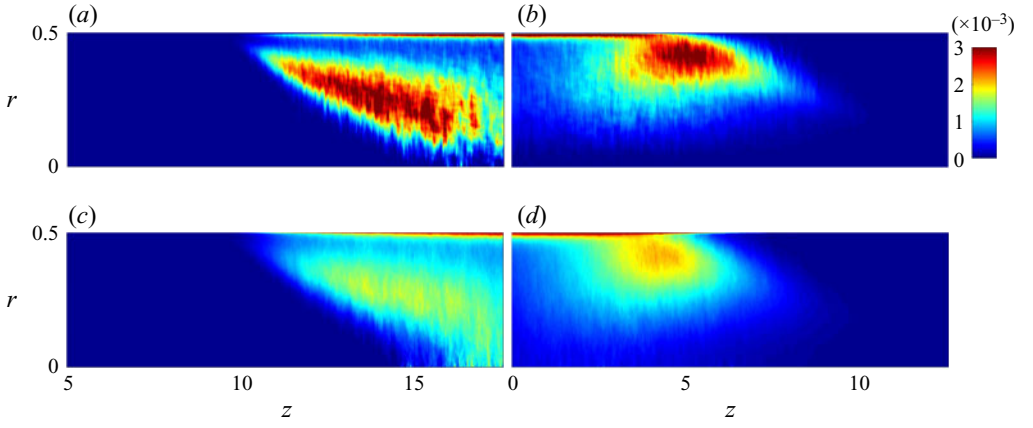

Figure 11. Azimuthally averaged production and dissipation in the r–z cross-section at the UF (a,c) and DF (b,d) for $Re = 25\,000$. The length in the vertical direction is stretched by a factor of eight in order to better display the distribution of the terms in the radial direction. In all panels, a pipe segment of $12.5D$ is shown. Here (a) P, UF; (b) P, DF; (c) ϵ, UF; (d) ϵ, DF.

4.1. *Production and dissipation of KE at the fronts*

As we showed in figures 7 and 8, the local transition at the DF is initiated near the pipe centre and close to the pipe wall at the UF. This observation can be more quantitatively shown by the energy budget analysis.

Following Song *et al.* (2017), we calculated the production and dissipation of the KE associated with velocity fluctuations approximately for the mean flow in the frame of reference comoving with the fronts, and the calculation is performed for the two fronts separately. Specifically, the production P and dissipation ϵ are calculated as

$$P = -\overline{u_i' u_j'} \frac{\partial \overline{u_i}}{\partial x_j}, \quad \epsilon = \frac{2}{Re} \overline{s_{ij} s_{ij}}, \tag{4.1a,b}$$

in which the overbar denotes the average over time and over the azimuthal direction in the moving frame of reference, the prime denotes the velocity fluctuation with respect to the mean flow $\overline{\boldsymbol{u}}(r, z)$, x_j denotes the spatial coordinates and s_{ij} is the fluctuating rate of strain defined as

$$s_{ij} = \frac{1}{2} \left(\frac{\partial u_i'}{\partial x_j} + \frac{\partial u_j'}{\partial x_i} \right). \tag{4.2}$$

Figure 11 shows our calculation of P and ϵ at the fronts for $Re = 25\,000$ in the $17.5D$ pipe. It can be seen that at the UF (figure 11a), production is highest in a thin layer near the pipe wall, as in the fully developed bulk region (Dimitropoulos *et al.* 2001; El Khoury *et al.* 2013), and in a more extended tilted region stretching from the near-wall region to the pipe centre, which extends more than seven diameters long in the axial direction. There is a gap with relatively lower production rate between these two regions. Similar distribution can be seen for the dissipation, except for that the dissipation rate in the extended tilted region is considerably lower than that in the near-wall region. At the DF, the production and dissipation rates are highest in a tilted region significantly far from the wall, and the downstream tip of this region protrudes into the laminar flow region close to the pipe centre (see figure 11b).

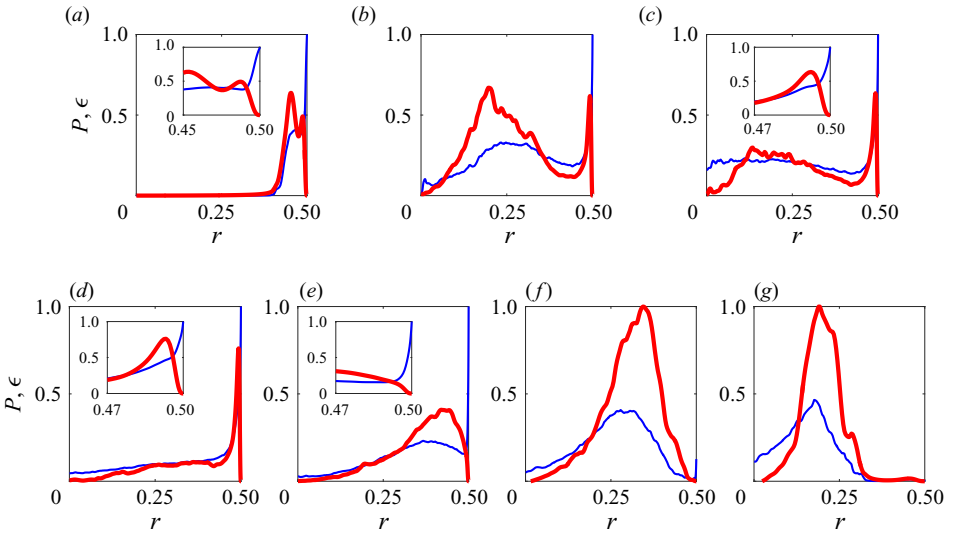

Figure 12. The profiles of production (bold red) and dissipation (thin blue) at several axial positions for the UF (*a–c*) and DF (*d–g*) for $Re = 25\,000$. The data are taken from that shown in figure 11. Here P and ϵ are normalised by the maximum of the two over the radius, i.e. $\max\{\max_r P, \max_r \epsilon\}$, at respective axial positions. The insets in panels (*a*,*c–e*) show the near-wall region. Here (*a*) $z = 10$; (*b*) $z = 15$; (*c*) $z = 17.5$; (*d*) $z = 0.5$; (*e*) $z = 5.0$; (*f*) $z = 7.5$; (*g*) $z = 10$.

The radial distributions of P and ϵ at the fronts can be more quantitatively shown by the radial profiles of the terms, see figure 12 for $Re = 25\,000$. The double-peak structure of P and ϵ at the UF can be clearly seen in figure 12(*b*,*c*), which was also reported by Wygnanski & Champagne (1973). Two peaks in P can be observed even at the upstream tip of the front where P and ϵ are very low (see figure 12*a*). The two peaks correspond to the near-wall region and the tilted region at the fronts as shown in figure 11(*a*,*c*), respectively. The flow at $z = 0.5$ for the DF is close to a fully developed turbulent flow. In viscous units, the peak of the production in figure 12(*d*) is approximately at $y^+ \approx 10$, which is at the bottom of the buffer layer, whereas the dissipation is dominant in the sublayer and peaks at the wall. The production nearly vanishes close to the pipe centre, whereas the dissipation is low but stays finite. These distributions of P and ϵ are similar to typical profiles for fully developed turbulent flow from the literature (Dimitropoulos *et al.* 2001; El Khoury *et al.* 2013). Figure 12(*e–g*) shows that as the axial position moves toward the tip of the DF, the region for P moves toward the pipe centre and at $z = 10$, the peak of P is approximately at $r = 0.2D$. Only a single peak can be observed at most part of the DF, in contrast to the UF.

The distributions of P and ϵ are consistent with our observation of the dynamics at the fronts illustrated by figures 7 and 8. At the UF, figure 8 shows that the transition is initiated at the tip of the front, which is close to the pipe wall, and the generated flow structures extend toward the pipe centre while being advected downstream by the faster flow. In this process, the turbulence strengthens presumably due to the stretching of the local mean shear (see evidence for the fronts of puffs by Holzner *et al.* (2013)). The turbulent KE will be produced during the spreading and strengthening of velocity fluctuations. Therefore, one can expect that a high-P region would appear as a tilted region connecting the near-wall region where the transition is initiated and the pipe centre where turbulence merges and fills the whole pipe cross-section (see the tilted red region in figure 11*a*).

With a strong production comes also a strong dissipation in the same region (see figure 11*c*), but the production outweighs the dissipation (see also figure 12*b*). The continuing transition and formation of turbulence at the tip (near pipe wall) and the spreading of the turbulence toward the pipe centre, counteracting the distorting effect of the advection of the local mean flow, together keep the characteristic shape of the front (see figure 6). At the DF, a similar transition scenario occurs as illustrated in figure 7. The distinction to the UF is that the local transition at the front tip is initiated near the pipe centre, and the generated turbulence spreads toward the pipe wall while being advected upstream relative to the front tip.

4.2. *The trend of the front speed as* $Re \to \infty$

Based on our observation of the dynamics at the fronts and the energy budget analysis, we propose that the trends of the front speeds will stay monotonic, i.e. the speed of the DF will keep increasing and the UF speed will keep decreasing as *Re* increases further.

As the tip of the fronts can be self-sustained, the transition at the tip must be triggered by velocity disturbances locally. As the adjacent flow is laminar, the disturbances that trigger the transition necessarily originate from the turbulent region. One possibility is that, at the UF, velocity disturbances close to the pipe wall, which propagate at low speeds due to the slow advection by the local mean flow, protrude from the turbulent region and trigger the transition. The generated turbulence locally feeds back the near-wall region with velocity disturbances, closing the self-sustaining cycle. It was proposed in the literature for puffs at low Reynolds numbers that low speed streaks protrude from the turbulent region at the UF and cause instabilities (Kelvin–Helmholtz by Shimizu & Kida (2009) and inflectional by Hof *et al.* 2010), sustaining the puffs. Our observation suggests that similar mechanisms may also take part at much higher Reynolds numbers. At the DF, disturbances close to the pipe centre, which propagate at high speed because of the advection of the mean flow, trigger the local transition at the front tip. Similarly, the generated turbulence feeds back the centre region with velocity disturbances. The self-sustainment is the reason why the front tips can be isolated without significantly affecting the kinematics of the fronts.

Positive $P - \epsilon$, referred to as the net production, is a signal for turbulence strengthening and therefore, presumably, can also be considered as a signature for the transition to turbulence at the front tip. It is expected that the net production would be very small at the early stage of the transition. Due to limited data for the energy budget analysis (we didn't save the velocity field frequently due to the large data size) and numerical errors, very low-level net production could be a false positive. Therefore, it is difficult to quantify the precise position of the transition at the front tip using this quantity in practice, because it is difficult to define a clear-cut threshold for the transition. Nevertheless, the regions enclosed by the contour lines with low contour levels in figure 13 can still be used to illustrate the trend of the position of the local transition at the front tip as *Re* increases. As can be seen, the region with net production moves closer to the pipe wall as *Re* increases at the UF, whereas it moves closer to the pipe centre as *Re* increases at the DF (especially, see the position of the noses of the contour lines shown in the insets of figure 13). This observation indicates that as *Re* increases, the position of the front tip where transition is initiated moves toward the pipe wall at the UF and moves toward the pipe centre at the DF. In other words, transition-inducing velocity disturbances are located closer to the pipe wall at the UF tip and are located closer to the pipe centre at the DF tip as *Re* increases.

In the following, we propose that the propagation speed of transition-inducing disturbances at front tips should be largely determined by the local mean flow speed. Studies have shown that, at least in fully developed turbulent channel and pipe flows, the

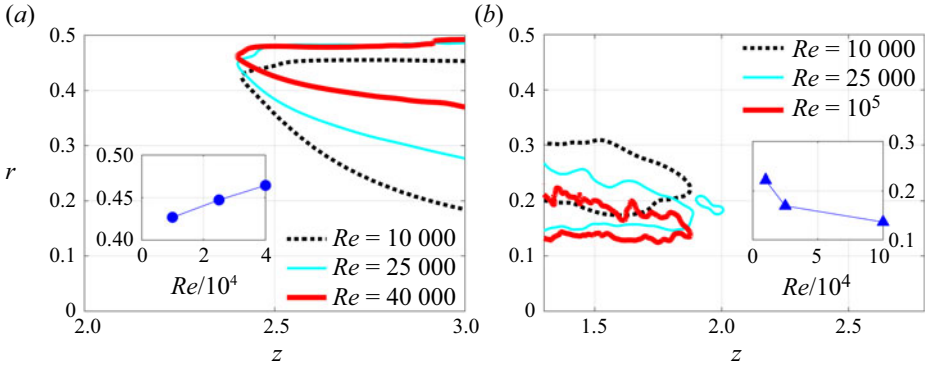

Figure 13. Contour lines of the net production $P-\epsilon$ at the front tip plotted in the r–z plane. (*a*) The contour level of 10^{-6} at the UF. (*b*) The contour level of 10^{-5} at the DF. The positions of the fronts are shifted in the axial direction such that the nose of these contour lines are approximately located at the same axial position for comparison. The ruggedness in some contour lines are due to the limited data for the energy budget analysis. The insets show the trend of the radial position of the nose of the contour lines, i.e. the leftmost point for the UF and the rightmost point for the DF.

advection speed of velocity fluctuations is close to (slightly slower than) the local mean flow speed except for the region very close to the wall with $y^+ \lesssim 10$, where the propagation speed of velocity fluctuations is considerably faster than the local mean flow (Del Álamo & Jiménez 2009; Pei *et al.* 2012; Wu & Moin 2012). Therefore, these studies suggest that the region where the propagation speed of velocity fluctuations significantly deviates from the local mean flow speed is the near-wall region where dissipation and production are large and strongly differ from each other (see the part of $r \gtrsim 0.48$ in figure 12*d*). While velocity fluctuations roughly follow the local mean flow in regions sufficiently far from the wall where production and dissipation are low or are nearly in balance, such as near the pipe centre and at the front tips. Consequently, the propagation speed of the transition-inducing velocity disturbances at the front tips should be largely determined by the local mean flow speed. Therefore, the trends in the radial position of the front tips shown in figure 13 suggest that the UF speed should decrease and the DF speed should increase as Re increases. This argument is consistent with our data in the considered Re range.

Although we do not have data at further higher Re, the trends can be expected to persist as Re increases further because of the following argument. It has been known that, as Re increases, the amplitude of disturbances needed to trigger turbulence decreases (Hof *et al.* 2003; Peixinho & Mullin 2007). Therefore, it can be expected that the transition at the UF tip would occur closer to the pipe wall as Re increases, because disturbances closer to the wall, which are in general of lower amplitudes, would be sufficient to trigger the transition. As a result, the speed of the UF would keep decreasing as Re increases. At the DF tip, the closer to the pipe centre the weaker the velocity disturbances (see figure 14 and the contours of $\sqrt{u_r^2+u_\theta^2}$ at the tip of the fronts in figure 7), and the faster the disturbances propagate due to the faster advection by the local mean flow. This distribution at the DF can be understood from another perspective. As figure 12(*e*–*g*) show, the dissipation outweighs the production near the pipe centre and the difference between the two terms is largest at the pipe centre. Thus, the turbulent KE can be expected to be lower when closer to the pipe centre. As weaker disturbances are sufficient to trigger transition as Re increases, it can be expected that the position where transition initiates at the DF tip would move toward the

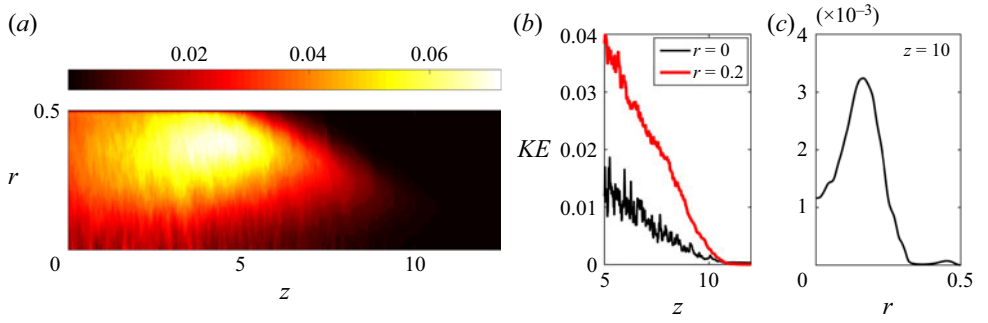

Figure 14. (*a*) The distribution of the azimuthally and temporally averaged turbulent KE ($KE = \overline{u_r'^2 + u_\theta'^2 + u_z'^2}$) in the z–r cross-section at the DF. (*b*) The distribution of KE along the pipe axis $r = 0$ (thin black) and at $r = 0.2$ (bold red). (*c*) The distribution of KE along the radius at $z = 10$.

pipe centre as Re increases, just as figure 13(*b*) suggests. Consequently, it can be inferred that the DF speed will keep increasing as Re increases.

As far as we can see, there is no mechanism that causes the DF to decelerate toward the bulk speed in the limit of $Re \to \infty$. The decreasing trend Wygnanski & Champagne (1973) reported at high Re should be attributed to the insufficient pipe length they used which did not even allow the basic laminar flow to fully develop before leaving the pipe exit, let alone the front speed. Their UF speed was not severely affected, because the developing blunted basic flow profile deviates from the parabolic profile most severely near the pipe centre, but only slightly near the pipe wall given the cylindrical geometry (see their figure 9). In fact, the decreasing trend of their DF speed supports our argument that the front speed is largely determined by the local flow speed at the front tip, given that the basic flow is more blunted (less developed) in their pipe as Re increases and consequently the local flow speed at the tip of the DF decreases.

It is interesting to note that, if the fittings (3.3) and (3.4) would apply in the limit of $Re \to \infty$, one would see that the DF speed would not approach exactly $2U$ and that the UF speed would not approach zero precisely. This would imply that, even at infinite Re, pipe flow would not become absolutely unstable (UF speed stays finite), and that the transition-inducing velocity disturbances would propagate slightly slower than the centreline velocity of the basic laminar flow.

4.3. *The flow structures at the two front tips*

Although the mechanism of the local transition at the front is still far from being clear, based on our analysis, we speculate that the transition mechanism at the UF is possibly different from that at the DF, because the transition occurs in the high shear region near the wall at the UF but in the low shear region near pipe centre at the DF. In the following, we show the flow structures at the two fronts.

Figure 15 visualises an instantaneous flow field at the front tips at $Re = 40\,000$ in the $5D$ pipe. The cross-stream velocity $\sqrt{u_r^2 + u_\theta^2}$ near the front tips are plotted in figure 15(*a*,*b*). The shown region is the z–r cross-section of a $1.7D$ pipe segment. The vertical lines mark the tip of the fronts, where, roughly, transition to turbulence is initiated (judged by eye). The azimuthally averaged streamwise velocity profiles, i.e. the local mean profiles, at the vertical lines are plotted in figure 15(*c*,*d*), which are nearly parabolic. Slight deviations can be observed very close to the wall at the UF and very close to the pipe centre at

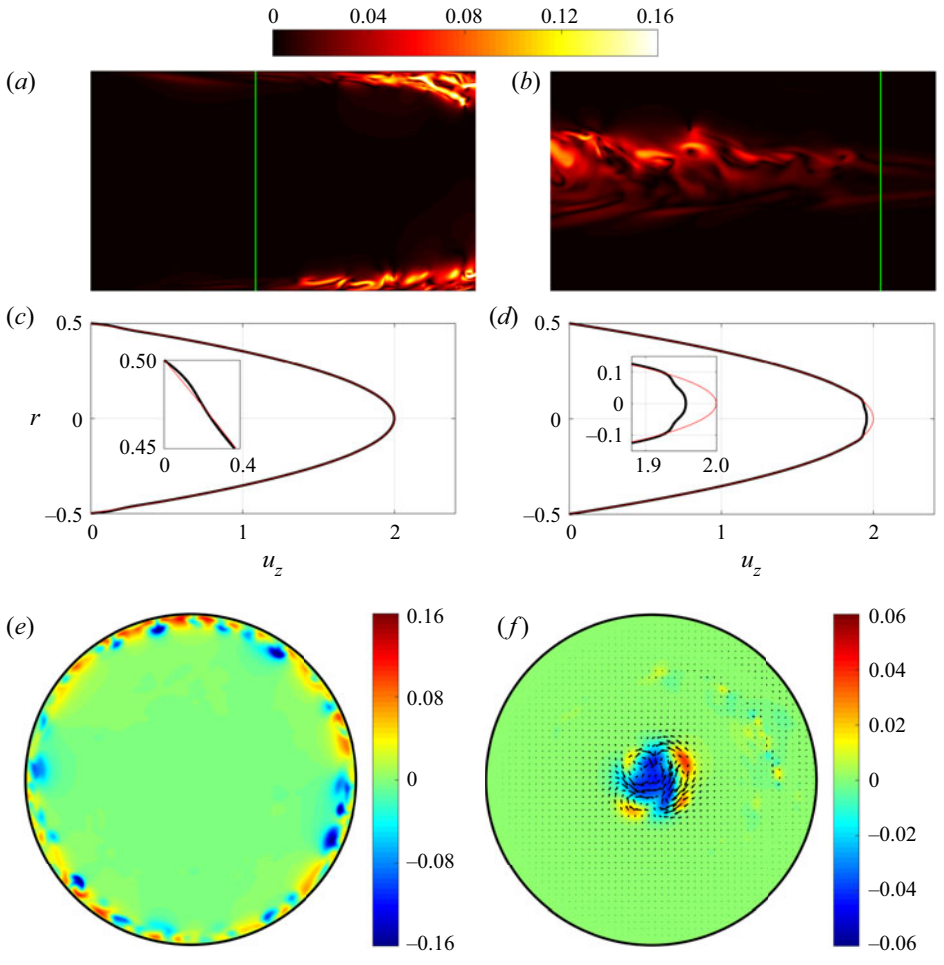

Figure 15. The cross-stream velocity $\sqrt{u_r^2 + u_\theta^2}$ in the z–r plane at the tip of the UF (*a*) and DF (*b*) at $Re = 40\,000$. (*c*,*d*) The profiles of the streamwise velocity, averaged in the azimuthal direction, at the positions marked by the two vertical lines in panels (*a*,*b*), respectively. (*e*,*f*) The contours of streamwise velocity deviated from the parabola in the r–θ plane at the positions marked by the two vertical lines in panel (*a*,*b*), respectively. In panel (*f*), the in-plane velocity is also plotted as a vector.

the DF. In other words, the mean flow modification by the turbulence at the front tips is very weak. Figure 15(*e*,*f*) show the contours of streamwise velocity components in the $r - \theta$ cross-section at the two vertical lines in figure 15(*a*,*b*). At the UF tip, it can be seen that high- and low-speed streaks with high azimuthal wavenumbers prevail close to the pipe wall, whereas the flow is nearly laminar elsewhere. Although the cross-stream velocity is weak (see the contour plots in figure 15*a*), the magnitude of the streaks can be as large as $O(0.1)$, i.e. streaks are the dominant flow feature at the tip of the UF. At the DF tip, flow structures (streaks and vortices) are concentrated close to the pipe centre. A low-speed region dominates at the pipe centre, but it can be seen that non-axisymmetric components are of substantial magnitude even in the streamwise velocity component, unlike the weak DF at much lower *Re* where axisymmetric flow dominates (see the analysis of turbulent puffs and localised invariant solutions in Ritter *et al.* (2018) at moderate *Re*).

5. Conclusion

By using a technique combining a moving frame of reference and an artificial damping, we were able to simulate the fronts at high Reynolds numbers in short periodic pipes. The applicability of this technique confirms that the fronts are locally self-sustained at high Reynolds numbers. We measured the global propagation speed of turbulent fronts up to $Re = 10^5$ in pipe flow, which is the highest Reynolds number considered so far, to the best of our knowledge. Our results presented scalings of the front speeds with Re in the widest Re range so far, see (3.3) and (3.4). The scaling of the UF speed is very close to that proposed theoretically for a model system by Barkley *et al.* (2015). The monotonically increasing trend of the DF speed is in stark contrast to the measurement of Wygnanski & Champagne (1973) above $Re \simeq 10\,000$, which was affected by the insufficient pipe length that didn't allow the flow to fully develop. Besides speed measurement, we also qualitatively discussed the mechanism that determines the front speed, which can be summarised by the following points.

(a) A strong front can keep a characteristic shape and speed because there is transition to turbulence continually occurring at the tip of the fronts (see figures 7 and 8 and the supplementary movies). The speed of the fronts should be determined by the radial position of the transition at the front tips.
(b) Our energy budget analysis showed that the position of the transition at the front tip moves towards the wall at the UF and moves towards the pipe centre at the downstream front, as figure 13 shows. This is consistent with the known fact that, as Re increases, the amplitude of perturbations needed to trigger pipe flow turbulence decreases.
(c) The trend in the front position suggests the monotonic trend in the front speed. The closer to the pipe wall, the lower the local flow speed at the UF tip. Therefore, one can expect a lower convection speed of the transition-inducing disturbances so that there is a lower UF speed. On the contrary, the closer to the pipe centre, the faster the local flow speed at the DF tip. Therefore, one can expect a faster convection of the transition-inducing disturbances so that there is a faster DF speed (approaching a limit).

Based on our analysis, we proposed that the speeds of both fronts would keep their respective monotonic trends as $Re \to \infty$. We also showed that the flow structures at the tips of the UF and DF, where local transition to turbulence continually occurs, are different. At the UF, the transition occurs in a high shear region near the pipe wall and the dominant structures exhibit high azimuthal wavenumbers, whereas the transition occurs in low shear region close to the pipe centre at the DF, exhibiting low azimuthal wavenumbers (but not axisymmetric). The different transition scenarios are possibly responsible for the asymmetry in the scaling of the two fronts. However, more quantitative studies are needed in the future for elucidating the instability and transition mechanisms at the front tip, which fundamentally determine the kinematics and flow structures of the fronts.

Supplementary movies. Supplementary movies are available at https://doi.org/10.1017/jfm.2021.1160.

Acknowledgements. We thank B. Hof, M. Avila and D. Barkley for insightful discussions on the topic over the years. We thank Y. Duguet for commenting on one version of our manuscript. The constructive comments from the anonymous reviewers are also acknowledged.

Funding. K.C. and B.S. acknowledge financial support from the National Natural Science Foundation of China under grant numbers 91852105 and 91752113 and from Tianjin University under grant number 2018XRX-0027. D.X. acknowledges the partial support from NSFC Basic Science Center Program for

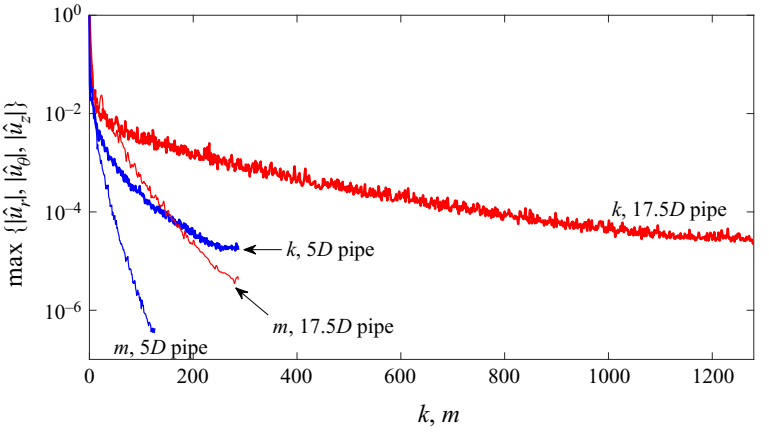

Figure 16. The velocity spectra for the DF in the 17.5D (red) and 5D (blue) pipes at $Re = 25\,000$ using the resolutions shown in tables 4 and 5. The horizontal axis represents the index of the Fourier modes (streamwise mode k or azimuthal mode m) and the vertical axis represents the modulus of the Fourier coefficient, maximised over three velocity components, radial direction and one of the two wavenumbers. Each data set is normalised by its maximum in order to compare the decrease in the spectra between different sets.

'Multiscale Problems in Nonlinear Mechanics' (no. 11988102). We acknowledge the computing resources from TianHe-2 at the National Supercomputer Centre in Guangzhou, where most of the simulations were performed. Part of the simulations were performed on TianHe-1(A) at the National Supercomputer Centre in Tianjin.

Declaration of interests. The authors report no conflict of interest.

Author ORCIDs.
Baofang Song https://orcid.org/0000-0003-4469-8781.

Appendix. Grid resolution

For the simulations in the 17.5D pipe, we used typical grid resolutions for DNS of fully turbulent flow (see e.g. Wu & Moin 2008; Ahn *et al.* 2015). Specifically, we used a grid spacing of $\Delta z^+ \approx 7.8$–9.6 in the streamwise direction and $0.5D^+\Delta\theta \approx 5.6$–$8.6$ in the azimuthal direction at the pipe wall, in which the normalisation is based on the viscous length unit evaluated for the fully turbulent flow at the respective Reynolds number; see table 4 for the detail. These resolutions can assure a decrease of no less than four orders of magnitude from the lowest to the highest Fourier mode in the velocity spectra, see an example for $Re = 25\,000$ in figure 16.

The resolutions for simulations in the 5D pipe are listed in table 5. The resolutions for the UF are nearly the same as those used for the 17.5D pipe. However, the resolutions for the DF are drastically lowered, see the numbers in the parentheses. As we explained in the main text, since we only need to simulate the tip of the DF, which is located in the low shear region near the pipe centre and exhibits larger flow structures than the small length scales in fully developed turbulent flow, we can resolve the flow using much lower resolution in both the streamwise and azimuthal directions. Figure 16 shows the comparison between the velocity spectra of a flow field for the DF simulated in the 17.5D and 5D pipes at $Re = 25\,000$. As can be seen, both resolutions give a decrease of more than four orders of magnitude in the velocity spectra and even a lower resolution could have been used for the simulation in the 5D pipe to obtain an equally well resolved flow field as that in the 17.5D pipe.

Re	$Re_\tau = \frac{u_\tau D}{\nu}$	Δr^+_{min}	Δr^+_{max}	$0.5D^+\Delta\theta$	Δz^+	N	M	K
5000	344	0.07	3.5	5.6	7.8	72	192	768
7500	490	0.06	3.8	8.0	8.4	96	192	1024
10 000	630	0.05	3.9	8.2	9.6	120	240	1152
17 500	1026	0.03	4.0	8.4	9.3	192	384	1920
25 000	1400	0.04	5.4	7.6	9.6	216	576	2560
40 000	2114	0.04	6.6	8.6	9.6	288	768	3840

Table 4. Grid resolutions used for simulations in the $17.5D$ pipe. Here Re_τ and the viscous length unit u_τ/ν are evaluated for the fully developed turbulent pipe flow at the same Reynolds numbers. Grid numbers in the radial, azimuthal and axial directions are given by N, M and K, respectively. Note that our Re_τ should be halved to compare with the literature in which usually the pipe radius is the reference length scale.

Re	$Re_\tau = \frac{u_\tau D}{\nu}$	Δr^+_{min}	Δr^+_{max}	$0.5D^+\Delta\theta$	Δz^+	N	M	K
17 500	1026	0.03	4.0	6.3 (16.8)	8.9 (8.9)	192	512 (192)	576 (576)
25 000	1400	0.04	5.4	6.9 (17.2)	9.1 (12.2)	216	640 (256)	768 (576)
40 000	2114	0.04	6.6	6.9 (17.3)	9.2 (16.5)	288	960 (384)	1152 (640)
60 000	3016	0.06	9.4	8.2 (24.7)	9.8 (15.7)	384	1152 (384)	1536 (960)
10^5	4714	— (0.04)	— (9.2)	— (28.9)	— (20.5)	— (384)	— (512)	— (1024)

Table 5. Grid resolutions used for simulations in the $5D$ pipe. Here Re_τ and the viscous length unit are evaluated for the fully developed turbulent pipe flow at the same Reynolds numbers. Grid numbers in the radial, azimuthal and axial directions are given by N, M and K, respectively. The numbers in the parentheses are for the DF.

References

Ahn, J., Lee, J.H., Lee, J. & Kang, J.-H. 2015 Direct numerical simulation of a 30R long tubrulent pipe flow at $Re_\tau = 3008$. *Phys. Fluids* **27**, 065110.

Barkley, D. 2016 Theoretical perspective on the route to turbulence in a pipe. *J. Fluid Mech.* **803**, P1.

Barkley, D., Song, B., Mukund, V., Lemoult, G., Avila, M. & Hof, B. 2015 The rise of fully turbulent flow. *Nature* **526**, 550–553.

Del Álamo, J.C. & Jiménez, J. 2009 Estimation of turbulent convection velocities and corrections to Taylor's approximation. *J. Fluid Mech.* **640**, 5–26.

Dimitropoulos, C.D., Sureshkumar, R., Beris, A.N. & Handler, R.A. 2001 Budgets of Reynolds stress, kinetic energy and streamwise enstrophy in viscoelastic turbulent channel flow. *Phys. Fluids* **13**, 1016.

Duguet, Y., Willis, A.P. & Kerswell, R.R. 2010 Slug genesis in cylindrical pipe flow. *J. Fluid Mech.* **663**, 180–208.

Durst, F. & Ünsal, B. 2006 Forced laminar to turbulent transition in pipe flows. *J. Fluid Mech.* **560**, 449–464.

El Khoury, G.L., Schlatter, P., Noorani, A., Fischer, P.F., Brethouwer, G. & Johansson, A.V. 2013 Direct numerical simulation of turbulent pipe flow at moderately high Reynolds numbers. *Flow Turbul. Combust.* **91**, 475–495.

Hof, B., De Lozar, A., Avila, M., Tu, X. & Schneider, T.M. 2010 Eliminating turbulence in spatially intermittent flows. *Science* **327**, 1491–1494.

Hof, B., Juel, A. & Mullin, T. 2003 Scaling of the turbulence transition threshold in a pipe. *Phys. Rev. Lett.* **91**, 244502.

Holzner, M., Song, B., Avila, M. & Hof, B. 2013 Lagrangian approach to laminar-turbulent interfaces. *J. Fluid Mech.* **723**, 140–162.

Kanazawa, T. 2018 Lifetime and growing process of localized turbulence in plane channel flow. PhD thesis, Osaka University.

LINDGREN, E.R. 1957 The transition process and other phenomena in viscous flow. *Ark. Fys.* **12**, 1–169.
LINDGREN, E.R. 1969 Propagation velocity of turbulent slugs and streaks in transition pipe flow. *Phys. Fluids* **12**, 418.
NISHI, M., ÜNSAL, B., DURST, F. & BISWAS, G. 2008 Laminar-to-turbulent transition of pipe flows through puffs and slugs. *J. Fluid Mech.* **614**, 425–446.
PEI, J., CHEN, J., SHE, Z.-S. & HUSSAIN, F. 2012 Model for propagation speed in turbulent channel flows. *Phys. Rev.* E **86**, 046307.
PEIXINHO, J. & MULLIN, T. 2007 Finite amplitude thresholds for transition in pipe flow. *J. Fluid Mech.* **582**, 169–178.
RINALDI, E., CANTON, J. & SCHLATTER, P. 2019 The vanishing of strong turbulent fronts in bent pipes. *J. Fluid Mech.* **866**, 487–502.
RITTER, P., ZAMMERT, S., SONG, B., ECKHARDT, B. & AVILA, M. 2018 Analysis and modeling of localized invariant solutions in pipe flow. *Phys. Rev. Fluids* **3**, 013901.
SHIMIZU, M. & KIDA, S. 2009 A driving mechanism of a turbulent puff in pipe flow. *Fluid Dyn. Res.* **41**, 045501.
SONG, B. 2014 Direct numerical simulation of transition to turbulence and turbulence control in pipe flow. PhD thesis, Gerog-August-Universität Göttingen.
SONG, B., BARKLEY, D., HOF, B. & AVILA, M. 2017 Speed and structure of turbulent fronts in pipe flow. *J. Fluid Mech.* **813**, 1045–1059.
WILLIS, A.P. 2017 The Openpipeflow Navier–Stokes solver. *SoftwareX* **6**, 124–127.
WILLIS, A.P. & KERSWELL, R.R. 2009 Turbulent dynamics of pipe flow captured in a reduced model: puff relaminarisation and localised 'edge' states. *J. Fluid Mech.* **619**, 213–233.
WU, X. & MOIN, P. 2008 A direct numerical simulation study on the mean velocity characteristics in turbulent pipe flow. *J. Fluid Mech.* **608**, 81–112.
WU, X. & MOIN, P. 2012 Direct numerical simulation of a 30R long turbulent pipe flow at R^+=685: large-and very large-scale motions. *J. Fluid Mech.* **698**, 235–281.
WYGNANSKI, I.J. & CHAMPAGNE, F.H. 1973 On transition in a pipe. Part 1. The origin of puffs and slugs and the flow in a turbulent slug. *J. Fluid Mech.* **59**, 281–335.